Enhanced Hall mobility in graphene-on-electronic-grade diamond

Applied Physics Letters

RESEARCH ARTICLE | JULY 06 2023

Enhanced Hall mobility in graphene-on-electronic-grade diamond

S. Majdi ; V. Djurberg ; M. Asad ; A. Aitkulova ; N. Suntornwipat ; J. Stake ; J. Isberg

Appl. Phys. Lett. 123, 012102 (2023)
https://doi.org/10.1063/5.0156108

AIP Publishing

Applied Physics Letters ARTICLE pubs.aip.org/aip/apl

Enhanced Hall mobility in graphene-on-electronic-grade diamond

Cite as: Appl. Phys. Lett. **123**, 012102 (2023); doi: 10.1063/5.0156108
Submitted: 26 April 2023 · Accepted: 17 June 2023 ·
Published Online: 6 July 2023

S. Majdi,[1,a)] V. Djurberg,[1] M. Asad,[2] A. Aitkulova,[1] N. Suntornwipat,[1] J. Stake,[2] and J. Isberg[1]

AFFILIATIONS

[1]Division for Electricity, Department of Electrical Engineering, Uppsala University, Box 65, 751 03 Uppsala, Sweden
[2]Terahertz and Millimetre Wave Laboratory, Department of Microtechnology and Nanoscience, Chalmers University of Technology, SE-412 96 Gothenburg, Sweden

[a)]**Author to whom correspondence should be addressed:** saman.majdi@angstrom.uu.se. **Tel.:** +46 18 4715854

ABSTRACT

The outstanding electronic properties of graphene make this material a candidate for many applications, for instance, ultra-fast transistors. However, self-heating and especially the detrimental influence of available supporting substrates have impeded progress in this field. In this study, we fabricate graphene-diamond heterostructures by transferring graphene to an ultra-pure single-crystalline diamond substrate. Hall-effect measurements were conducted at 80 to 300 K on graphene Hall bars to investigate the charge transport properties in these devices. Enhanced hole mobility of 2750 $cm^2\ V^{-1}\ s^{-1}$ could be observed at room-temperature when using diamond with reduced nitrogen (N_s^0) impurity concentration. In addition, by electrostatically varying the carrier concentration, an upper limit for mobility is determined in the devices. The results are promising for enabling carbon–carbon (C-C) devices for room-temperature applications.

The excellent electronic characteristics of graphene are highly desirable for a new generation of electronics, energy storage, and spintronics.[1–3] In particular, electronic applications have evolved following the introduction of the large-scale chemical vapor deposition (CVD) method.[4] Nevertheless, technological obstacles still set limits of device reproducibility, properties, and performance. The graphene-based device preparation process is complex and crucial for achieving good charge transport properties.[5–7] Earlier studies have presented several issues,[8,9] e.g., self-heating or phonon scattering depending on the chosen substrate for devices.[10,11] Silicon dioxide, SiO_2/Si,[7] is the most commonly used substrate for graphene due to the substrate engineering advances.[7,12,13] However, the low thermal conductivity of SiO_2 (≈1.4 W $m^{-1}\ K^{-1}$)[14] and Si (145 W $m^{-1}\ K^{-1}$) at room-temperature (RT) restricts the superior current-carrying capacity of graphene. By selecting SiC (0001), Pallecchi *et al.* improved the carrier mobility (μ) of epitaxial-grown graphene as high as 11 000 $cm^2\ V^{-1}\ s^{-1}$ at 0.3 K.[15]

Using sp^3 carbon, diamond, as a substrate for 2D sp^2 carbon, graphene, is compelling due to diamond's electrical and chemical stability, high thermal conductivity, and excellent charge transport properties.[16] Moreover, diamond has high optical phonon energy ($\hbar\omega_{LO} = 165$ meV) and a low surface trap density due to its nonpolar and inert nature, highly important properties for limiting the intrinsic scattering in graphene on a host substrate. Graphene exhibits very high carrier mobility (>10^4 $cm^2\ V^{-1}\ s^{-1}$) at RT.[9,17] Hu *et al.* predicted the charge carrier density (n) of graphene to be up to 7×10^{12} cm^{-2} on diamond (111) substrates using density functional theory calculations.[18] Surface-treated [(H:O:F:N) terminated] (100) single-crystalline diamond (SCD)[19] and diamond-like carbon (DLC)[20] have been previously investigated as alternative substrates for graphene with an obtained $\mu \sim 300$ $cm^2\ V^{-1}\ s^{-1}$. Recently, we have demonstrated enhanced graphene field-effect transistor (FET) performance on electronic-grade SCD. High-frequency (54 GHz) device operation was achieved, indicating a high substrate-limited mobility.[21]

Here, we fabricate graphene-diamond heterostructures by transferring high-quality monolayer graphene on top of an electronic-grade SCD (G-ESCD) substrate. The electrical properties of these devices were investigated through Hall-effect measurements across a wide temperature (T) range, 80–300 K. For comparison, the same measurements were applied to optical-grade SCD (G-OSCD). These two substrates differ mainly in the concentration of substitutional N_s^0 impurities. A significant increase in Hall hole mobility ($\mu_{H,h}$) in the G-ESCD devices could be observed compared to previous studies on similar heterostructures.[19,20] The results are encouraging for

developing stable, all-carbon devices technology for high-power and high-frequency electronics.[22,23]

A set of free-standing commercially available SCD substrates, optical and high-purity electronic grade, were chosen for this study. The diamond substrates (5×5 mm and 500 μm thick) were homoepitaxially grown in the (100) direction using microwave plasma-assisted CVD by Element Six Ltd.[16] The nitrogen impurity level, for the electronic-grade sample, is below 5×10^{14} cm^{-3} ($N_s^0 < 5$ ppb), which is determined by electron paramagnetic resonance measurements, whereas the optical-grade sample contains a significantly higher N_s^0 concentration (≈50 ppb). Atomic force microscopy (AFM) was performed using a PSIA XE-150 in contact mode to investigate the surface morphology.

Prior to device fabrication, substrates were cleaned in strongly oxidizing solutions to remove any residual surface conductivity. The samples were boiled in a graphite etch (HNO_3:H_2SO_4:$HClO_4 = 1$:1:1) for 40 min at 180–200 °C and oxygen-terminated in an oxygen plasma for 60 s.[24] Commercially available monolayer CVD graphene grown by Graphenea Inc. was transferred onto the diamond substrates. The graphene Hall bar structures were fabricated through the following steps [also shown in Fig. 1(a)]. To avoid contact between the electron-beam resist and the graphene film, a 5-nm thick Ti/TiO_2 protection layer is used. Subsequently, a graphene mesa is defined by plasma dry etching. The protection layer is removed by wet-etching in the contact area, and Ohmic electrodes, Ti/Pd/Au (1/15/285 nm), are deposited by evaporation and patterned using liftoff. A 5-nm thermally oxidized Al_2O_3 seed layer is formed followed by an 18-nm top layer Al_2O_3 applied by atomic layer deposition (ALD) on top of the graphene channel after the removal of the remaining TiO_2. In addition, a gate-pad is created by deposition of a Ti/Au (100/300 nm) layer on the G-ESCD devices (this final step was absent in processing G-OSCD devices). Electron-beam lithography (EBL) is employed in all the patterning steps.

Hall-effect measurements were used to characterize the charge carrier transport in the G-D devices. Figure 1(b) shows the Hall setup and the graphene Hall bar structure on the diamond substrate. We use an AC Hall system based on two Signal Recovery 7265 DSP lock-in amplifiers.[25] An electromagnet applies a magnetic field between ±0.5 T perpendicular to the electric field. The sample is mounted on a sample holder in a liquid nitrogen-cooled Janis ST-300MS vacuum cryostat. The Hall voltage was measured using a 6-terminal configuration at temperatures between 80 and 300 K. The temperature was monitored using a LakeShore 331 T-controller with a calibrated TG-120-CU-HT-1.4H GaAlAs diode sensor in good thermal contact with the sample.

The surface morphology of the diamond substrates was observed across a 5×5 μm area using scanning AFM. Uniform and smooth substrate surfaces with an average roughness of $R_a \sim 0.2$ nm and $R_a \sim 0.3$ nm were observed by the AFM scans for electronic and optical-grade diamond, respectively.

The sheet resistivity (ρ) and n for G-ESCD and G-OSCD devices are plotted against T as shown in Fig. 2(a). In the case of G-ESCD devices, the gate electrode was held at ground potential. The sheet resistivity shows very little temperature dependency, a small increase from 765 to 1060 Ω/sq for G-ESCD, while the G-OSCD devices are almost independent of the T, 505 to 522 Ω/sq over the whole temperature range (see the inset). Figure 2(a) also reveals a difference of one order of magnitude in the carrier concentration, e.g., $\sim 4.50 \times 10^{13}$ and $\sim 2.25 \times 10^{12}$ cm^{-2} measured for the G-OSCD and G-ESCD, respectively, at RT.

The $n = B/eR_{xy}$ is determined by applying an out-of-plane magnetic field (B) in a Hall bar geometry. Knowing W and L (width and length of the Hall bar), the longitudinal resistance R_{xy} (constant for small B) and $\rho = R_{xy}(W/L)$ are determined. Hall mobility is calculated as $1/en\rho$. A high $\mu_{H,h}$ (2750 ± 50 cm^2 V^{-1} s^{-1}) is observed in G-ESCD devices, almost ten times higher compared with similar graphene devices on optical-grade diamond. The Hall characterization reveals that the mobility is dominated entirely by p-type conduction. Measured $\mu_{H,h}$ shows comparatively weak or no temperature dependence in both types of devices [Fig. 2(b)]. For instance, at low temperature (80 K), the $\mu_{H,h}$ measured in G-OSCD devices is 320 cm^2 V^{-1} s^{-1} slightly decreased to ∼290 cm^2 V^{-1} s^{-1} at RT. This is comparable to

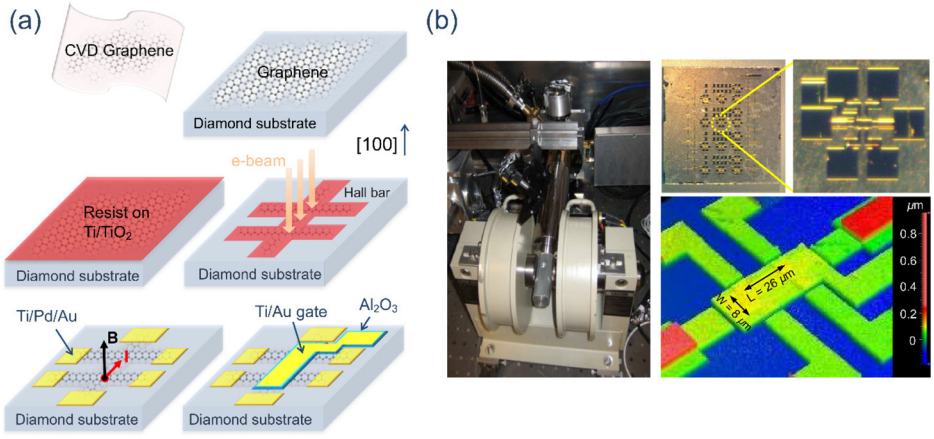

FIG. 1. (a) Schematic illustration of the graphene-on-diamond device fabrication process. Top left: CVD graphene (Graphenea) was transferred on top of the (100) SCD. The graphene was covered by Ti/TiO_2 and then by resist. Graphene Hall bars are defined by a mesa using EBL followed by dry etching. Electrodes are formed through evaporation and liftoff. Al_2O_3 is deposited by ALD as the gate dielectric prior to Ti/Au gate contact formation on top of the channel. (b) The Hall-effect system used in the experiment is shown in the left. Top view photography of the graphene-diamond (G-D) Hall bars taken by optical microscopy (up) and 3D coherence scanning interferometry (ZYGO).

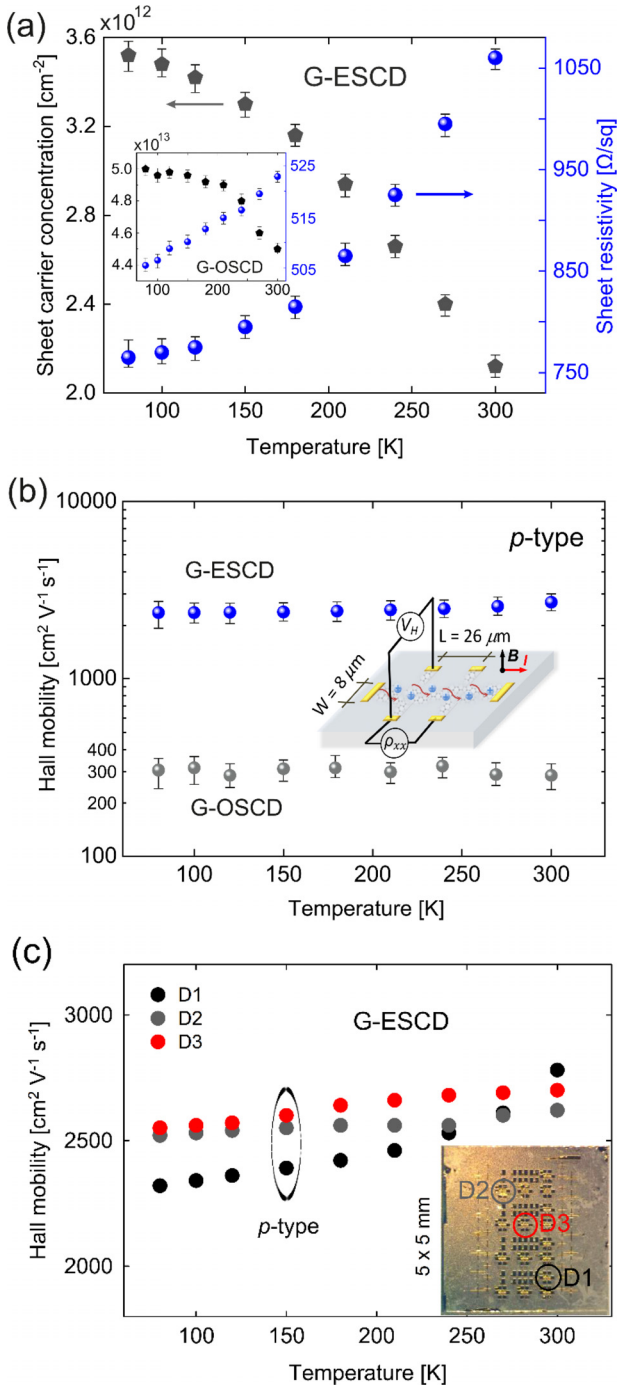

FIG. 2. (a) Temperature dependent Hall-effect characteristics of G-D devices. The insets show the results for graphene on the optical-grade diamond substrate. The blue circles indicate ρ, and the gray pentagons show n represented by the right and left axis, respectively. (b) Temperature dependent Hall mobility together with the schematic and dimensions of the Hall bars of the two types of G-D heterostructures. (c) Comparison of mobility in different G-ESCD devices (D1-D3) as a function of temperature. Error bars in (a) and (b) indicate the standard variation between different devices on the same sample for a specific temperature.

the mobilities measured in graphene deposited on (H:O:F:N)-terminated diamond at RT (221 $cm^2\ V^{-1}\ s^{-1}$ on H-terminated SCD).[19] The measured values are summarized in Table I.

Irregularities in the 2D film strongly affect the charge transport properties of graphene. However, by placing graphene on a supporting substrate, we enter the regime where the intrinsic properties of graphene are shadowed by the quality of the substrate. Here, we have used similar graphene films as investigated in a previous study performed by Asad *et al.*,[21] indicating a high quality also reflected by the observed results (high frequency and saturation velocity). Comparison between different devices on the same substrate shows relatively low variation in performance for specific temperature. Figure 2(c) shows mobility results for three devices (D1-D3) in G-ESCD with less than 8% local deviation. The fact that different devices, separated by millimeter distances on the same diamond substrate, exhibit similar performance is a proof of the homogeneity of the graphene film.

Both optical and electronic-grade diamond substrates have the same thermal conductivity (~2000 W/mK) and function as a heat-sink for the graphene film. In addition, as the AFM measurement reveals, the surface roughness of the diamond substrates is comparable as care has been taken to ensure a high surface quality. Moreover, previous in-depth studies of the intrinsic electronic properties in SCD by the time-of-flight technique confirm very low impurity concentration ($N_s^0 \leq 10^{-13}\,cm^{-3}$), charged impurities ($\leq 10^{-10}\,cm^{-3}$), and a high carrier mobility in the electronic-grade substrates.[26,27] As indicated by the substantially lower carrier density observed in G-ESCD devices, the lower background impurity concentration of the substrate is likely the main reason.[28,29] However, the observations show that the mobility of carriers in our graphene sheets is insensitive to variations in temperature, and, hence, that influence of electron-phonon scattering is small. Asad *et al.*[21] estimate a high velocity saturation $\sim 3.2 \times 10^7$ cm s^{-1} in G-ESCD FET devices at RT attributed to the high phonon energies in diamond (165 meV). This means that the effect from scattering by optical phonons at the surface and subsurface could be suppressed.

In the diffusive regime, disorder sources, e.g., impurities and interaction with charges in the surrounding substrate, act as scattering centers in graphene. To investigate the dominating scattering mechanisms limiting the mobility, we performed further measurements, focused on the G-ESCD devices with higher quality. By varying the gate voltage (V_g) from −5.0 to +6.0 V, we determine the sheet carrier concentration change in the graphene channel. The data collected [Figs. 3(a)–3(c)] confirm a Fermi level shift through the Dirac point when $V_g \sim$ 3.5 V and, thus, determine the charge neutrality point (CNP). Away from the CNP ($n > 10^{12}\,cm^{-2}$), the ρ increases slightly with increasing T [Fig. 3(a)]. This could possibly be explained by the formation of electron and hole puddles in graphene near the Dirac point.[30] The temperature dependency of Hall coefficient (R_H) is similar to the sheet resistivity, as shown in the inset of Fig. 3(b). The sign of the R_H reflects the majority charge carriers in the sample, and if $R_H < 0$, the conduction corresponds to electrons, while $R_H > 0$ designates p-type or hole conduction [Fig. 3(b)]. Hence, three clear regions are distinguished, as shown in Fig. 3(c), indicating hole majority transport, intrinsic ambipolar conduction ($R_H = 0$), and electron majority transport as V_g is shifted. The mobility dependency of T is shown in the inset of Fig. 3(c) for three different V_g (−5, 0, and 6 V). A maximum electron mobility $\mu_{H,e} \sim 1680 \pm 30\,cm^2\ V^{-1}\ s^{-1}$ is achieved at RT and $V_g = 6$ V. Figure 3(d) shows measured μ as a function of n for the

TABLE I. Hall-effect results for different G-D devices.

	$n \times 10^{12}$ cm^{-2}		ρ (Ω/sq)		$\mu_{H,h}$ (cm^2 V^{-1} s^{-1})	
Device	80 K	300 K	80 K	300 K	80 K	300 K
G-ESCD	3.5 ± 0.3	2.3 ± 0.1	765 ± 55	1060 ± 50	2320 ± 60	2750 ± 50
G-OSCD	50.1 ± 0.9	45.2 ± 1.1	505 ± 35	522 ± 20	320 ± 17	290 ± 14
G-SCD[19]	6.5		4392		221	
G-DLC[20]	11		1702		313	

entire temperature range (100–300 K). We observe an increase in the mobility as carrier density decreases, at all T, which is most likely due to short-range scattering.[31]

The contribution of longitudinal acoustic (LA) phonon scattering $\rho_{LA} = \frac{\pi D_A^2 k_B}{4e^2 \rho_F v_s^2 v_F^2} T$ can be neglected considering that the magnitude of the mobility limited by the LA phonon scattering ($\sim 10^5$ cm^2 V^{-1} s^{-1})[32] is much larger than the mobilities seen in our case. Here, ρ_F, v_F, v_s, D_A, and k_B are two-dimensional mass density, Fermi velocity of graphene, the LA phonon velocity, deformation potential, and the Boltzmann constant, respectively.[33] A simple model for how carrier transport in graphene is affected by variations in measured n was presented by Hwang *et al.*[31] By assuming long-range scattering, which can be attributed to ionized impurity Coulomb scattering from ions in the substrate, and short-range scattering, generally associated with defects in the graphene itself, the following relation for sheet resistivity σ^{-1} is found when the residual conductivity at the Dirac point is neglected:

$$\sigma^{-1} = (ne\mu_c)^{-1} + \rho_s. \quad (1)$$

Here, $\mu_c \propto 1/n_{ion}$ is the density-independent mobility due to long-range scattering, ρ_s is the resistivity from short-range scattering, and n is varied electrostatically by applying a gate voltage. The expression (1) is then fitted to the measured conductivity $\sigma(V_g)$ and the best least squares fit yield values for μ_c and ρ_s. The results of the measurements on the G-ESCD sample are illustrated in Figs. 4(a) and 4(b). We find an upper limit for μ_c approximately ~2500 and ~3000 (cm^2 V^{-1} s^{-1}) and ρ_s values ~45 and ~92 (Ω) at 100 and 300 K, respectively.

In our case, the resistivity from short-range scattering is comparable to findings from other studies, e.g., for graphene grown on h-BN[33] and SiO_2[34] [Fig. 4(c)]. However, the μ_c due to the long-range Coulomb scattering is lower, indicating that the limiting factor is the concentration of ionized impurities and surface charge traps in the diamond substrate. This fact can also explain the increase in graphene channel mobility between optical and electronic-grade devices. As shown in Fig. 4(c), when using other substrates (h-BN and SiO_2) to

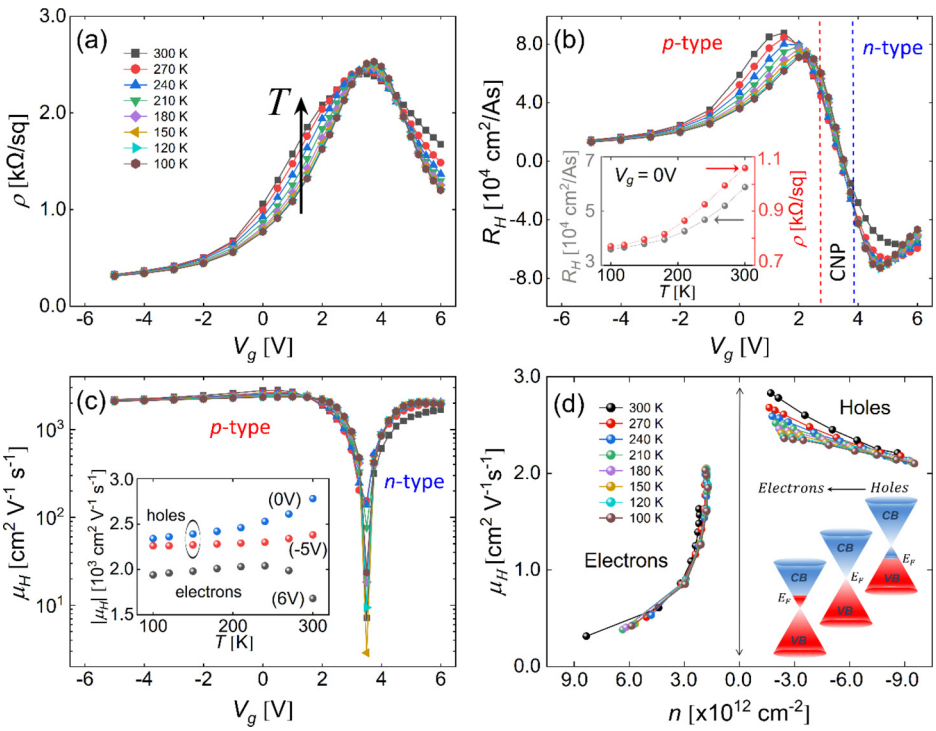

FIG. 3. (a)–(c) ρ, R_H, and calculated μ_H as a function of gate voltage at T between 100 and 300 K and B = 0 T. (d) Mobility dependence of carrier density in G-ESCD devices at various T. Insets: (b) R_H and the sheet resistivity dependency of T at $V_g = 0$ V, (c) mobility variation as a function of T for three different V_g (−5, 0, and 6 V), and (d) schematic illustration of the Fermi level shift around the Dirac point.

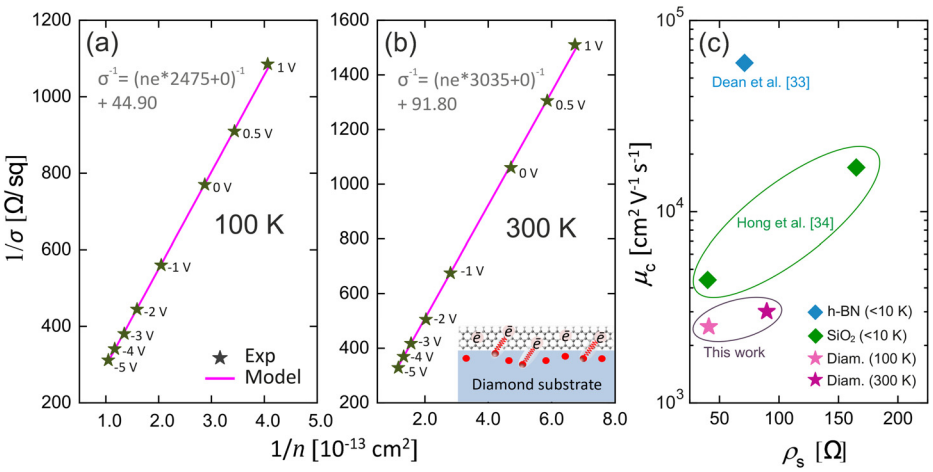

FIG. 4. (a) and (b) Measured graphene resistivity together with a fit from Eq. (1) assuming a combination of short- and long-range scattering for 80 and 300 K, respectively. (c) Calculated μ_c and ρ_s from this study. For comparison, data from graphene on boron nitride[33] and silicon oxide[34] substrates are also included.

achieve high mobility, the measurements were performed at very low temperatures to minimize the effect of phonon scattering. Having high optical phonon energy, the scattering rate is limited in diamond at high temperatures. However, further investigation is needed to fully map the scattering process in such heterostructures. For example, we have only considered the impurity below the graphene channel, and, hence, no consideration has been made regarding the impact from the top cap layer (TiO_2) since all devices were prepared under similar conditions.

In summary, we have fabricated graphene-on-diamond heterostructures. The electronic properties of graphene grown on ultra-pure electronic-grade SCD Hall bars were systematically investigated. A sheet carrier concentration of approximately around 2.25×10^{12} cm^{-2} in G-ESCD devices was measured, whereas a high carrier mobility $\sim$2750 cm^2 V^{-1} s^{-1} was observed, almost constant across the whole temperature range 80–300 K. The results were compared with optical-grade SCD substrates containing a higher amount of background nitrogen. Further investigation with a focus on G-ESCD reveals that charge transport in graphene films is less affected by both long-range and short-range Coulomb interactions originating from near-surface ionized defects in the diamond and graphene interface. Our results indicate that selecting high-purity diamond improves the electronic transport properties of graphene films transferred under otherwise identical conditions. A high mobility in the graphene, together with the very high thermal conductivity in diamond, is very beneficial for devices where heating is an issue, e.g., for high-frequency graphene transistors at room-temperature. This could provide a platform for the development of stable RT C-C electronics.

The authors acknowledge the Swedish Research Council (VR, Grant No. 2018-04154) and Swedish Energy Agency (Grant No. 44718-1) for the financial support. This work was also supported in part by the European Union's Horizon 2020 Research and Innovation Programme (Grant No. 881603).

AUTHOR DECLARATIONS

Conflict of Interest

The authors have no conflicts to disclose.

Author Contributions

Saman Majdi: Conceptualization (equal); Data curation (equal); Formal analysis (equal); Investigation (equal); Project administration (equal); Validation (equal); Writing – original draft (equal). **Viktor Djurberg:** Formal analysis (equal); Investigation (equal); Writing – review & editing (equal). **Muhammad Asad:** Formal analysis (equal); Investigation (equal); Writing – review & editing (equal). **Aisuluu Aitkulova:** Investigation (equal); Writing – review & editing (equal). **Nattakarn Suntornwipat:** Validation (supporting); Writing – review & editing (equal). **Jan Stake:** Funding acquisition (equal); Project administration (equal); Supervision (equal); Validation (equal); Writing – review & editing (equal). **Jan Isberg:** Funding acquisition (equal); Investigation (equal); Supervision (equal); Validation (equal); Writing – review & editing (equal).

DATA AVAILABILITY

The data that support the findings of this study are available from the corresponding author upon reasonable request.

REFERENCES

[1]K. S. Novoselov, A. K. Geim, S. V. Morozov, D. Jiang, Y. Zhang, S. V. Dubonos, I. V. Grigorieva, and A. A. Firsov, Science **306**, 666 (2004).
[2]K. S. Novoselov, V. I. Fal'ko, L. Colombo, P. R. Gellert, M. G. Schwab, and K. Kim, Nature **490**, 192 (2012).
[3]W. Han, R. K. Kawakami, M. Gmitra, and J. Fabian, Nat. Nanotechnol. **9**, 794 (2014).
[4]A. Zurutuza and C. Marinelli, Nat. Nanotechnol. **9**, 730 (2014).
[5]J. Lee, Y. Kim, H.-J. Shin, C. Lee, D. Lee, C.-Y. Moon, J. Lim, and S. Chan Jun, Appl. Phys. Lett. **103**, 103104 (2013).
[6]J. Lee, S. Lee, and H. K. Yu, Coatings **7**, 218 (2017).
[7]X. Liang, B. A. Sperling, I. Calizo, G. Cheng, C. A. Hacker, Q. Zhang, Y. Obeng, K. Yan, H. Peng, Q. Li, X. Zhu, H. Yuan, A. R. Hight Walker, Z. Liu, L. Peng, and C. A. Richter, ACS Nano **5**, 9144 (2011).
[8]D. Y. Jung, S. Y. Yang, H. Park, W. C. Shin, J. G. Oh, B. J. Cho, and S.-Y. Choi, Nano Convergence **2**, 11 (2015).
[9]J. H. Gosling, O. Makarovsky, F. Wang, N. D. Cottam, M. T. Greenaway, A. Patanè, R. D. Wildman, C. J. Tuck, L. Turyanska, and T. M. Fromhold, Commun. Phys. **4**, 30 (2021).
[10]S. Sonde, F. Giannazzo, C. Vecchio, R. Yakimova, E. Rimini, and V. Raineri, Appl. Phys. Lett. **97**, 132101 (2010).

[11]S. V. Koniakhin, O. I. Utesov, I. N. Terterov, and A. V. Nalitov, Phys. Rev. B **95**, 045418 (2017).
[12]R. Lukose, M. Lisker, F. Akhtar, M. Fraschke, T. Grabolla, A. Mai, and M. Lukosius, Sci. Rep. **11**, 13111 (2021).
[13]K. I. Bolotin, in *Graphene*, edited by V. Skákalová and A. B. Kaiser (Woodhead Publishing, 2014), pp. 199–227.
[14]T. Yamane, N. Nagai, S. Katayama, and M. Todoki, J. Appl. Phys. **91**, 9772 (2002).
[15]E. Pallecchi, F. Lafont, V. Cavaliere, F. Schopfer, D. Mailly, W. Poirier, and A. Ouerghi, Sci. Rep. **4**, 4558 (2014).
[16]J. Isberg, J. Hammersberg, E. Johansson, T. Wikström, D. J. Twitchen, A. J. Whitehead, S. E. Coe, and G. A. Scarsbrook, Science **297**, 1670 (2002).
[17]F. Giannazzo, S. Sonde, R. L. Nigro, E. Rimini, and V. Raineri, Nano Lett. **11**, 4612 (2011).
[18]W. Hu, Z. Li, and J. Yang, J. Chem. Phys. **138**, 054701 (2013).
[19]F. Zhao, T. Thuong Nguyen, M. Golsharifi, S. Amakubo, K. P. Loh, and R. B. Jackman, J. Appl. Phys. **114**, 053709 (2013).
[20]F. Zhao, A. Afandi, and R. B. Jackman, Appl. Phys. Lett. **106**, 102108 (2015).
[21]M. Asad, S. Majdi, A. Vorobiev, K. Jeppson, J. Isberg, and J. Stake, IEEE Electron Device Lett. **43**, 300 (2022).
[22]Q. Yuan, C.-T. Lin, and K. W. A. Chee, APL Mater. **7**, 030901 (2019).
[23]J. Yu, G. Liu, A. V. Sumant, V. Goyal, and A. A. Balandin, Nano Lett. **12**, 1603 (2012).
[24]K. K. Kovi, S. Majdi, M. Gabrysch, and J. Isberg, Appl. Phys. Lett. **105**, 202102 (2014).
[25]N. Suntornwipat, M. Gabrysch, S. Majdi, D. J. Twitchen, and J. Isberg, Phys. Rev. B **94**, 035408 (2016).
[26]S. Majdi, M. Gabrysch, K. K. Kovi, N. Suntornwipat, I. Friel, and J. Isberg, Appl. Phys. Lett. **109**, 162106 (2016).
[27]S. Majdi, V. Djurberg, N. Suntornwipat, M. Gabrysch, and J. Isberg, Adv. Theory Simul. **4**, 2000103 (2021).
[28]J.-H. Chen, C. Jang, S. Xiao, M. Ishigami, and M. S. Fuhrer, Nat. Nanotechnol. **3**, 206 (2008).
[29]P. Avouris, Nano Lett. **10**, 4285 (2010).
[30]J. Martin, N. Akerman, G. Ulbricht, T. Lohmann, J. H. Smet, K. von Klitzing, and A. Yacoby, Nat. Phys. **4**, 144 (2008).
[31]E. H. Hwang, S. Adam, and S. D. Sarma, Phys. Rev. Lett. **98**, 186806 (2007).
[32]E. H. Hwang and S. Das Sarma, Phys. Rev. B **77**, 115449 (2008).
[33]C. R. Dean, A. F. Young, I. Meric, C. Lee, L. Wang, S. Sorgenfrei, K. Watanabe, T. Taniguchi, P. Kim, K. L. Shepard, and J. Hone, Nat. Nanotechnol. **5**, 722 (2010).
[34]X. Hong, K. Zou, and J. Zhu, Phys. Rev. B **80**, 241415 (2009).